# Molecular dynamics simulations to understand the mechanical behavior of functional gradient nano-gyroid structures

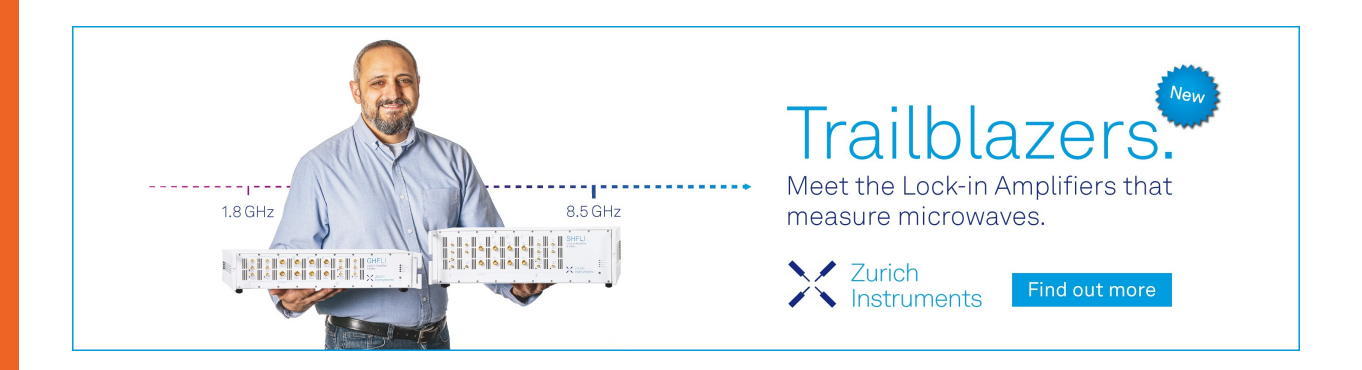
Cite as: J. Appl. Phys. 132, 135109 (2022); https://doi.org/10.1063/5.0102297 Submitted: 08 June 2022 • Accepted: 31 August 2022 • Published Online: 05 October 2022







Rui Dai, Dawei Li, Wenhe Liao, et al.





# Molecular dynamics simulations to understand the mechanical behavior of functional gradient nano-gyroid structures

Cite as: J. Appl. Phys. **132**, 135109 (2022); doi: 10.1063/5.0102297 Submitted: 8 June 2022 · Accepted: 31 August 2022 · Published Online: 5 October 2022







Rui Dai,<sup>1</sup> Dawei Li,<sup>2</sup> Wenhe Liao,<sup>2</sup> Haofan Sun,<sup>1</sup> Yunlong Tang,<sup>3</sup> and Qiong Nian<sup>1,a)</sup>

### **AFFILIATIONS**

- <sup>1</sup>School of Engineering for Matter, Transport and Energy, Arizona State University, Tempe, Arizona 85287, USA
- <sup>2</sup>School of Mechanical Engineering, Nanjing University of Science and Technology, Nanjing, Jiangsu 210094, China
- <sup>3</sup>Department of Mechanical & Aerospace Engineering, Monash University, Clayton, Victoria 3800, Australia

### **ABSTRACT**

Gyroid structure, a nature inspired cellular architecture, is under extensive exploration recently due to its structure continuity, uniform stress distribution under compression, and stable collapse mechanism during deformation. However, when combining with a functional gradient, the Gyroid structure can perform much different mechanical behavior from its homogeneous counterpart. Herein, bottom-up computational modeling is performed to investigate the mechanics of functional gradient nano-gyroid structure made of copper (Cu). Our work reveals that its mechanical properties degrade with a density that is much slower than those of homogeneous gyroid structure. The scaling of yield strength  $(\sigma_y)$  to the relative density  $(\rho')$  for the functional gradient gyroid structure is in the factor of 1.5. Moreover, the layer-by-layer collapsing mechanism yields significantly better mechanical energy absorption ability. This study not only leads to insightful understanding of the deformation mechanisms in nonuniform gyroid structures but also promotes the development of the functional gradient cellular materials.

Published under an exclusive license by AIP Publishing. https://doi.org/10.1063/5.0102297

#### I. INTRODUCTION

Cellular materials, including stochastic foams and architected lattice structures, are under extensive exploration in recent years, due to their attractive mechanical property and light weight. They are used as either single component or building blocks for complex structures, demonstrating their exceptional properties in enormous engineering applications. As one type of cellular material, naturalinspired architectures commonly possess porous and hierarchical levels and are evolved to have compelling multifunctional properties.2 For instance, the single gyroid minimum geometry is one nature-inspired architecture, which is a member of the triply periodic minimal surface (TPMS) family.3 One example of the natural gyroid structure can be found on the wing of the butterfly, as shown in Fig. 1(a), which is fascinating subject to the increasing interest in structural color, photonics, and optics. 1,4-7 As an architected porous structure and being simultaneous lightweight and strong, it can potentially be made as a thin film for battery electrodes applied in electronic sectors, or as a bulk part with high impact energy absorption capability employed in applications ranging from automobile to aerospace, personnel protection, <sup>10</sup> packaging, etc.

Several different gyroid-based cellular materials are recently fabricated to further understand the structure and biomimetics from nature. 11,12 For example, Abueidda et al. 11 fabricated polymeric Gyroid cellular and found that such structures have comparable mechanical properties to other TMPS family members. In addition, with the advances of additive manufacturing (AM), such as high-resolution AM and laser lithography techniques become available, it is even feasible to fabricate 3D gyroid cellular with feature resolution down to the scale of a few to few hundred nanometers. For example, Gan et al. 4 demonstrated that using the optical two-beam lithography technique to replicate Gyroid photonic nanostructures in the butterfly Callophrys Rubi up to several hundred nanometers and potentially aid in investigating biomimetic structures.

The rapid developments in fabricating nanolattices have also continuously extended material space and redefined the mechanical limit. Given that the size of the material structure decreases below

a)Author to whom correspondence should be addressed: giong.nian@asu.edu

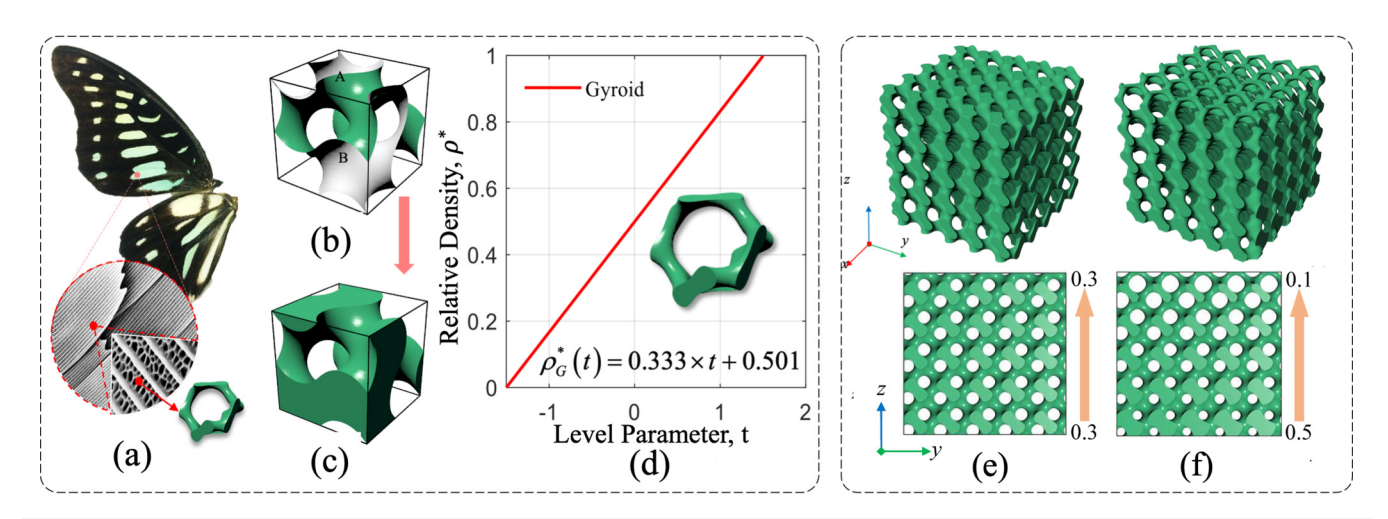


**FIG. 1.** Nanoscale gyroid structure modeling and compression deformation process: (a) microstructure of butterfly wings; gyroid surface (b) close to be solid gyroid structure (c); (d) the relationship between level parameter t and relative density; (e) and (f) are the nano-gyroid structures with gradients 0 and 4, respectively.

the micro-scale, many architectural cellular materials made of single-crystalline metal exhibit the size effect. It can tremendously alter the mechanical and electrical properties compared to those cellular materials fabricated in the macroscale. Thus, the study of nanosized architectural cellular materials is essential. With the size effect, nanoscale cellular materials exhibit unique and unparalleled mechanical properties, known as "the smaller the stronger," e.g., high deformability,<sup>2,13</sup> superior recoverability with brittle material, 14 and ultrahigh effective strength. 13 The gyroid-like structures are also studied in nanoscale to demonstrate their exceptional mechanical properties. For example, Park and Lee<sup>15</sup> show that the nano-gyroid yields an unusually high shear modulus to Young's modulus ratio, which is twice larger than conventional bulk materials. In addition, they found that Young's modulus (E) and shear modulus (µ) of nanoscale TPMS structures change with the relative density and size at different rates for different morphologies. 16 Qin et al. 17 investigated the mechanics of fundamental Gyroid graphene structures and revealed that although 3D graphene has exceptional mechanical strength and stiffness, its mechanical properties decrease with density in a much faster speed than those of polymer foams. Moreover, various experiments and simulations demonstrate nanoscale gyroid-like TPMS structures display a relatively uniform stress distribution under compression leading to a stable collapse mechanism since they possess no discontinuities and avoid stress concentration during deformation. <sup>10,11,18,19</sup> In addition, Li et al. <sup>20</sup> studied the Cu/Ni gyroid composite structure finding that the effective modulus is higher than the sum of two phases. Zhang et al.<sup>21</sup> investigated the gyroid glass structure demonstrating its distinct mechanical properties due to the lacking of global-plasticity. Despite those studies mentioned above, to the authors' best knowledge, nevertheless, there is limited research concerned with the mechanical properties of nanoscale functionally graded gyroid structures, and their impact energy properties is yet to be studied.

To provide a reliable understanding of the mechanical properties of nanoscale functional graded gyroid structures, we performed MD simulations on a group of nanoscale functional graded gyroid structures made of copper (Cu). A single crystal Cu lattice comprise of nanotwinned structural elements has significantly improved mechanical strength compared to the equivalent bulk material.<sup>22</sup> However, it is still unknown how the size effect, which becomes critical under 100 nm scale, impacts the mechanical properties of nanolattices. In this study, it is observed the functional graded gyroid structure of Cu exhibits a layer-by-layer collapse deformation mechanism, and the energy absorption linearly depends on the gradient level. The layer-by-layer collapse behavior reflects a highly programmable potential, e.g., stiffness and strength. Noteworthy, when the gradient distinction is large enough, surface effects may become dominant, resulting in nonlinear behavior. In addition, it is found that unlike the conventional homogeneous Gyroid structure, the power coefficient relation for the yield strength of functional gradient gyroid structures is ~1.5 yielding a stretch dominant behavior. This work will be instrumental in understanding the mechanical response of gradient gyroid cellular on a nanoscale and developing a new class of stable nanosized metamaterials.

### **II. METHODS**

### A. Uniform and gradient gyroid generation

The gyroid is one of the most widely studied TMPS structures, discovered in the 1970s by NASA scientist Alan Schoen and designed for lightweight, high-strength materials discovery. The gyroid structure is stably present in nature on a nanoscale, such as the microstructure of butterfly wings, as shown in Fig. 1(a). The Gyroid surface can use a triply periodic function to express its spatial form, as shown in Fig. 1(b) and Eq. (1),

$$F_{G}(x, y, z) = \sin\left(2\pi \frac{x}{L}\right) \times \cos\left(2\pi \frac{y}{L}\right) + \sin\left(2\pi \frac{y}{L}\right) \times \cos\left(2\pi \frac{z}{L}\right) + \sin\left(2\pi \frac{z}{L}\right) \times \cos\left(2\pi \frac{x}{L}\right) - t, \quad (1)$$

where L is the cubic unit cell edge length and the level parameter t is a variable and determines the volume fractions in the regions separated by the surface. The gyroid structure can be established in Fig. 1(c). Different volume fractions of the gyroid structure can be obtained by varying the parameter t, and its relationship to relative density  $\rho^{23}$  is shown in Fig. 1(d). In Figs. 1(e) and 1(f), the homogeneous and functional gradient gyroid structures have a size parameter of  $10 \times 43 \times 43$  nm and a same relative density of 0.3. The relative density  $\rho'$  is defined as  $\rho/\rho_s$ , where  $\rho$  is the density of the gyroid lattice and  $\rho_s$  is the density of the base material. The maximum density minus the minimum density divided by 0.1 is defined as the structure gradient  $\eta$ . For example, the nano-gyroid structure gradient of uniform density is 0 and the density range of 0.1–0.5 is 4.

### B. Molecular dynamics (MD) simulation for nano-gyroid structure

MD simulations are performed using the LAMMPS package<sup>24</sup> with embedded-atom (EAM) potential parameterized by Mishin *et al.*<sup>25</sup> to study the gradient gyroid cellular structure and investigate their elastic response. The parameterization of the adopted EAM potential is obtained using the ab-initio electronic calculations. Moreover, the potential utilized is proved to be capable of accurately capturing the essential deformation behavior after analyzing the stress–strain relation, atomic relaxation, and  $\gamma$  surface for {111} shear. It makes the EAM potential feasible to study large atomic systems compared with *ab initio* electronic calculations.<sup>26</sup>

To elucidate the mechanical properties of the gradient effect, all the MD simulations are performed with structure gradients ranging from 0 to 4. FCC bulk copper (edge length around 40 nm) with over 2 million atoms is generated as a single crystal oriented all along the (100) direction. Subsequently, extra atoms are removed according to Eq. (1) resulting from the uniform gyroid and gradient nano-gyroid cellular structures containing around 1 680 000 atoms and a relative density of 0.1-0.5, respectively. Periodic boundary conditions (PBCs) are applied along with all three directions of the nanolattice cell. If lattice deformation behaviors along the z-direction are to be considered, only two units are created along the x-direction. Initially, we performed the MD simulations within the Isothermal-Isobaric (NPT) ensemble for 800 ps with a time step of 1 fs. Such treatment is supposed to relax the system while letting the structure reaches its equilibrium state. During the equilibrium process, the total temperature was kept at 300 K, and the pressure along all three axial directions was kept at zero. After that, the equilibrated structure was compressed along the z-direction with a compression strain up to 65% of the original length. The deformation-controlled uniaxial compression possesses a strain rate of 109 s<sup>-1</sup> and the pressure component perpendicular to the compression direction was controlled, maintaining the uniaxial compression condition. Viral stress is used to calculate the atom stress, and the method is described as the following. The atomic stress tensor  $S_{ii}^{\alpha}$  at atom  $\alpha$  is calculated by the following equation, where i and j act as x, y, or z indicating six different components of the stress tensor:

$$S_{ij}^{\alpha} = \frac{1}{2} m^{\alpha} v_i^{\alpha} v_j^{\alpha} + \sum_{\beta=1}^n r_{\alpha\beta}^j f_{\alpha\beta}^i. \tag{2}$$

 $m^{\alpha}$  and  $v^{\alpha}$  are the mass and velocity of atom  $\alpha$ ;  $r_{\alpha\beta}$  and  $f_{\alpha\beta}$  are the distance and force between atoms  $\alpha$  and  $\beta$ . Once the stress tensor is obtained, the equivalent stress of nano-gyroid structures is calculated based on von Mises stress described as

$$\sigma_{von\_Mise} = \sqrt{\frac{1}{2}[(\sigma_{xx} - \sigma_{yy})^2 + (\sigma_{yy} - \sigma_{zz})^2 + (\sigma_{zz} - \sigma_{xx})^2 + 6(\sigma_{xy}^2 + \sigma_{yz}^2 + \sigma_{zx}^2)]}.$$
 (3)

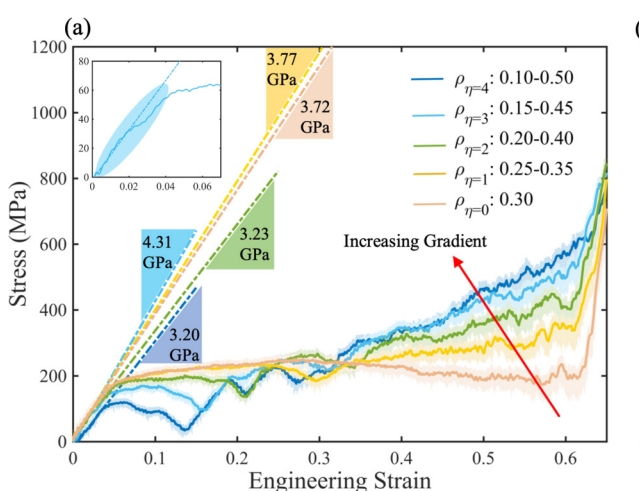
Here,  $\sigma_{ij} = \frac{1}{V_0} \sum_{\gamma=1}^{n} S_{ij}^{\gamma}$ , where  $V_0$  is the initial volume of the system. Figure 2 shows the calculated stress-strain curve of the nano-gyroid architectures.

## **III. RESULTS AND DISCUSSION**

# A. Mechanical properties of homogeneous and gradient gyroid

We performed MD simulations to study the compression deformation of the nano-gyroids on different relative densities up to the strain of 0.65, as shown in Fig. 2. At around 60% deformation, the gyroid nanolattices begin to fail and lose their loading capacity. The compressive stress-strain curve of nano-gyroid structures with gradient densities is shown in Fig. 2(a). As observed, depending on relative density levels, the compression response varies, exhibiting a distinct mechanical behavior with macroscale bulk Cu lattice structures. Specifically, a linear deformation is first observed with

compression strain ranging from 2.0% to 4.3%, followed by the distinct plastic yielding, then another linear region and plastic yielding stage. This alternative behavior is never observed in pure bulk crystals. After each yielding, we observed a plateau in the flow stress followed by failure via layer densification. However, unlike the graded one, there is no apparent cyclic-reinforced region for the uniform gyroid model ( $\eta = 0$ ). Figure 2(b) presents schematic diagrams of the von Mises stress distribution along the z-direction for  $\eta = 0$  and  $\eta = 4$  model, respectively. The uniform Gyroid nano lattice exhibits a homogeneous stress concentration, and every layer of the structure is simultaneously compressed and deformed throughout the compression before being densified. At the same time, the gradient one fails layer by layer, providing a continuous decay in mechanical stiffness, which indicates the potential of the gradient nano-gyroid structure performing as a programmable architecture for larger deformation to be applied in broad areas, e.g., mechanical energy absorption, damage tolerance, and recoverability.



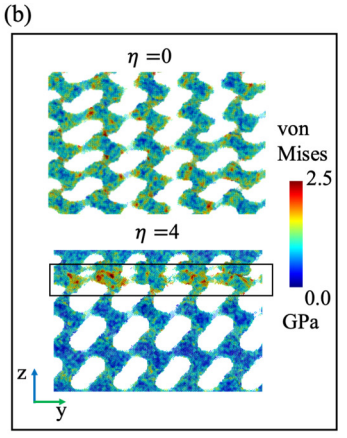


**FIG. 2.** (a) Compressive stress–strain curves of  $\langle 100 \rangle$  Gyroid lattice structures with different gradients. (b) Schematic diagram of the atomic von Mises stress distribution for  $\eta=0$  and  $\eta=4$ , respectively. The red areas indicate the yielding regions. A black rectangular is a marker of the collapse region on top layers for the  $\eta=4$  model.

Another intrigue phenomenon we find is Young's modulus, for traditional structure, the effective Young's modulus is defined with the gradient of the first 2% to 4% deformation region. However, unlike conventional homogeneous cellular gyroid structure, there is no linear deformation part, no matter how small the initial region is, which originates from the inhomogeneous nature. The inset image in Fig. 2(a) is a representative stress–strain response for  $\eta=3$  model.

Young's modulus is derived from the most significant gradient within the starting 2% to 4% deformation region. Among the five models, the  $\eta=3$  model (relative density 0.15–0.45) possesses the highest stiffness. According to the Gibson–Ashby theory,<sup>27</sup> a power coefficient relationship can be used to correlate the relative density and the total effective modulus, which is  $E=C\rho^n$ , where C is a constant, n is a power coefficient. Since the relative density of all the

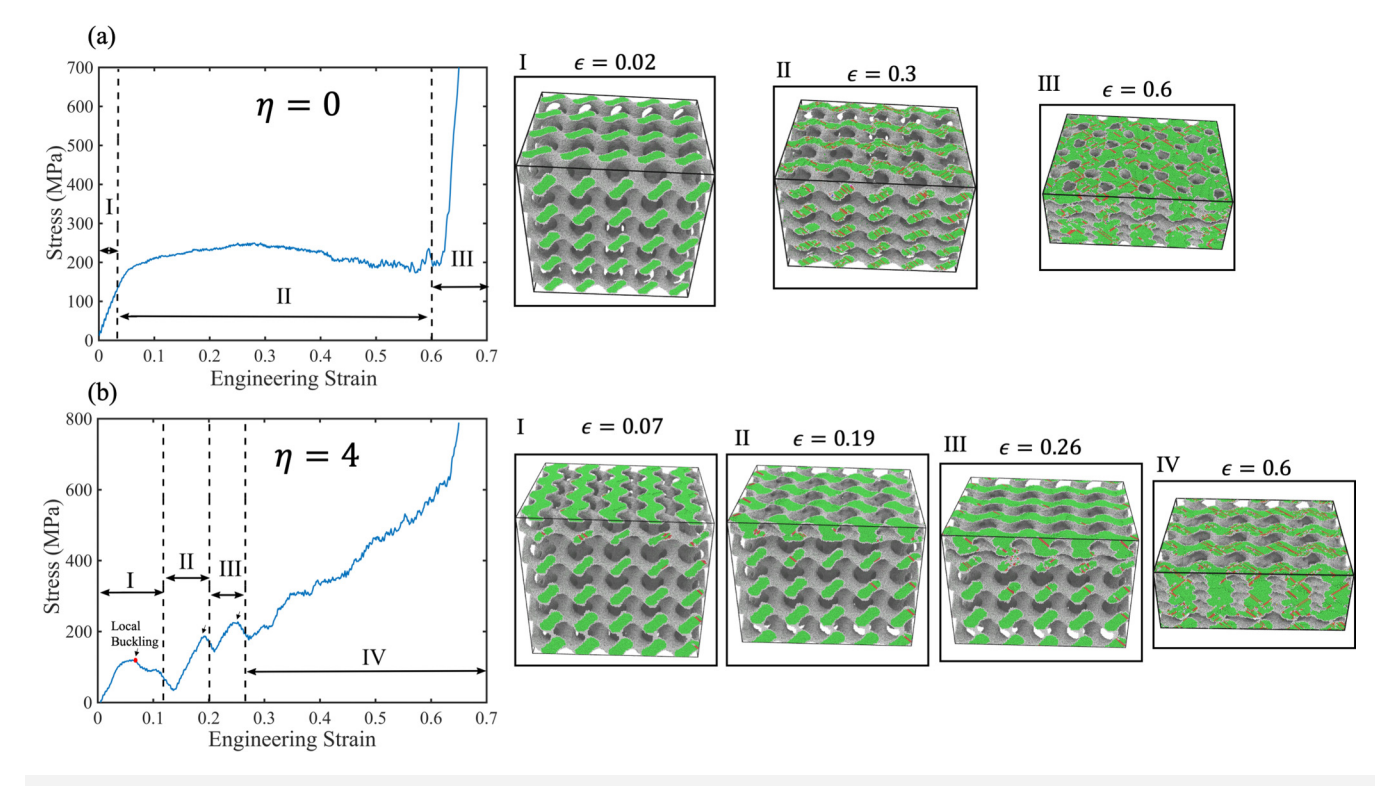


FIG. 3. Engineering stress-strain curve of gradient 0 and gradient 4 model with the (100) nanolattice (a) and (b).

graded gyroid structures is the same, their effective Young's modulus should be in a similar level. Due to the high strain rate, the stiffness vibration is acceptable.

To connect the mechanical response with atomic-scale deformation, we provide the compression deformation of  $\eta=0$  and  $\eta=4$  structures at several levels of overall strain, from 0.02 to 0.3 shown in Fig. 3. The homogeneous and the gradient nano-gyroid cellular structures exhibit completely different deformation responses. For the homogeneous gyroid model, the compression process is divided into three stages (I) elastic stage, (II) plastic stage, and (III) densification.

The compression of gradient gyroid structures can be divided into four stages containing: (I) (II) (III) elastic-plastic deformation stage, (IV) densification. The densification in a gradient structure leads to a rapid increase in stress above the yield stress, which occurs due to the continuous densification within the unit cell compared to the uniform structure. Noteworthy, for the  $\eta = 4$  model, there is a buckling near the 0.1 strain region, which is not observed in the uniform structure due to the small aspect radio to be approximate as a thin truss. The buckling position is marked red on the stress and strain plot in Fig. 3(b). After the buckling point, a distinct steep drop of the stress dramatically decreases the mechanical strength and releases the local stress concentration on the top layer region. The obtained stress-strain relation can then be used to analyze the yield behavior. Figure 4(a) is an example of the local buckling for one of the ligaments. Figure 4(b) indicates during compression, the dislocation mainly occurs in the node region. Figures 4(a) and 4(b) collectively yields that the stress drop is attributed to the local bucking of the ligament. Unlike the homogeneous gyroid structure, which deforms, fails uniformly and therefore, yields a steady stress and strain behavior, the graded one performs a gradual increasing strength. It's worth to mention, even in the stochastic carbon based cellular architectures, 28,29 there are no such linear densification stage either. It is concluded that the gradual increasing of the strength is a result of the internal gradient of the cellular lattice structure.

Considering the nanoscale essence of the gradient gyroid architecture, the size effect plays a determining role in the variation of the mechanical properties, which is rarely elucidated in

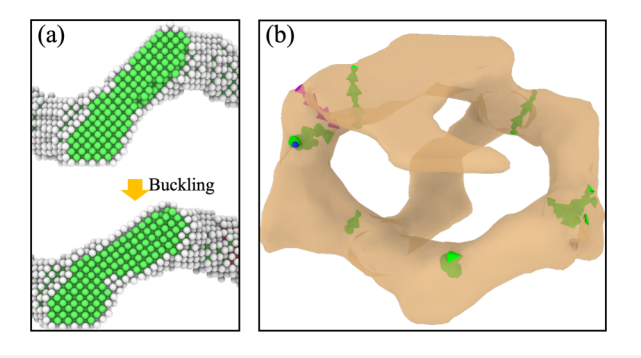


**FIG. 4.** (a) Schematic illustration of a local buckling for a single ligament at 7% effective engineering strain; white atoms are the surface atoms, while green atoms are the body atoms. (b) Dislocation distribution in a single Gyroid lattice unit. The arrows indicate Burgers vector.

experiments due to the difficulties in preparing the sample and conducting the measurement in such a small scale. Also, two questions are naturally proposed in this small scale and aroused great interest: (1) the mechanism dominating the plastic deformation process, and (2) how the yield stress varies with increasing gradient level. To gain further insights into the size effect of the gradient nano-gyroid architecture to answer the above questions, yield stress vs the different gradient level for the same size of the nano-gyroid copper structure is plotted in Fig. 5. Herein, the yield strength is defined as the 3% average stress after reaching the maximum stress point on each densification stage for the uniaxial compression. It is seen that different gradient level leads to a gradual increase in the maximum compressive strength but a decrease in the minimum compressive strength. Moreover, the yield strength is stabilized by decreasing the gradient. For the following part, the surface effect is introduced to interpret the size effect on the yield behaviors of the gradient nano-gyroid.

To further study the behavior of yield strength, Khaderi et al. <sup>19</sup> demonstrate that for the yield strength at low relative density, the gyroid lattice architecture can be idealized as a 3D framework of beams possessing a uniform cross-sectional area, and the yield strength can be expressed as

$$\sigma_{\rm Y} = \frac{\sigma_{\rm S}}{6\sqrt{2}} \left(\frac{d}{L}\right)^n = 0.438\sigma_{\rm S} \bar{\rho}^{\frac{n}{2}},\tag{4}$$

where  $\bar{\rho}=\frac{3\pi}{16\sqrt{2}}(\frac{d}{L})^2$ ,  $\sigma_S$  is the yield strength of the parent material. The strut length L is related to the unit-cell size a by  $a=2\sqrt{2}L$ , and d is the average diameter of the strut. According to  $J_2$  flow theory  $\sigma_S=0.01E_s$ . For pure copper with the [100] orientation, the Young's modulus is 67.1 GPa. Figure 5(a) plots out the yield strength vs the relative density. Since each layer possesses distinct relative density, fitting the yield strength with the relative density for each layer yields a geometry factor n equal to 3, and the resulted scaling factor n/2 is 1.5. For the conventional gyroid-type lattice structure, the scale factor is 3. Paccording to Gibson-Ashby's law, a scale factor  $\sim$ 3 indicates a bending dominant structure, and a scale factor  $\sim$ 1 yields a stretching dominant structure. The graded gyroid lattice therefore shows a stretching dominant behavior, signaling less modulus and strength decay when reducing the relative density than the uniform gyroid lattice architecture, thus leading to better mechanical performance.

For a single ligament, according to the study by Zhou *et al.*,<sup>30</sup> the size effect arising from the surface stress follows a 1/D scaling, where D is the diameter of the strut. Therefore, the yield strength can be written in the form of the friction coefficient  $\mu$ , while  $\tau$  and C are two constants in the unit of  $J/m^2$  and  $N/m^2$ , respectively,

$$\sigma_{y} = -\alpha \frac{2\tau}{D} + C,\tag{5}$$

$$\alpha = \frac{\sqrt{1 + \mu^2} - 3\mu}{\sqrt{1 + \mu^2} - \mu} \ . \tag{6}$$

As shown in Fig. 1, the structure is approximated as the repeating unit for a single reduced strut but with different inclined

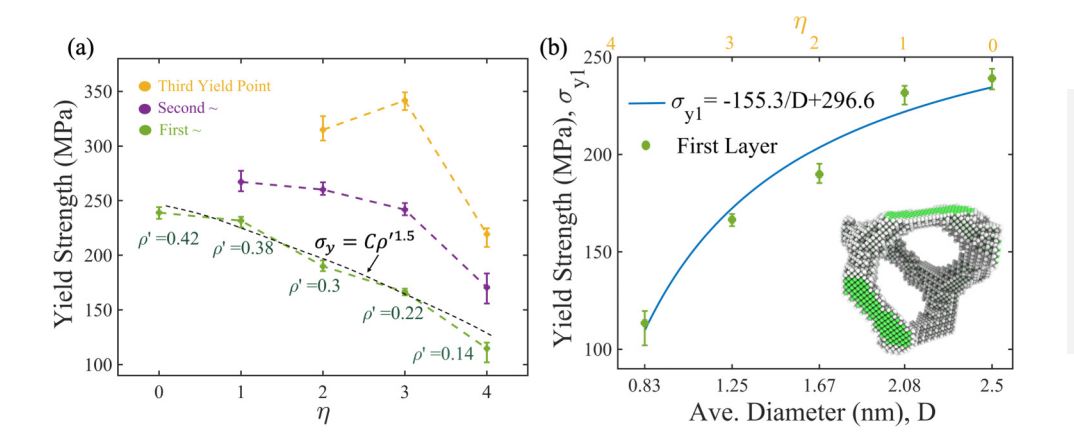


**FIG. 5.** (a) Compressive yield strength at different densification levels as a function of gradient level. (b) Yield strength of the first layer,  $\sigma_{y1}$  vs the minimum diameter of the gradient gyroid architecture. The curve demonstrates the theoretical prediction for the yield strength of gradient nano-gyroid lattice. Inset image is the layer unit structure of the gyroid model.

angles for the regular gyroid lattice. Therefore, the total yield stress is then taken to be proportional to the yield strength of the strut model result, and yield stress is expressed as  $\sigma_Y = -\frac{C_1}{D} + C_2$ .  $C_1$  and  $C_2$  are the constants, which depend on the number of struts and the alignment angles. Average the strut length for each layer region, D is obtained as shown in Fig. 5(b). Fitting the above equation with the obtained yield strength for the gradient nano gyroids, we find  $C_1$  is 155.3 N/m and  $C_2$  is 296.6 MPa. The analytical formula in Eq. (5) is compared with molecular dynamics simulations as a function of strut diameter for the gyroid lattice as shown in Fig. 5(b), the agreement is excellent.

# B. Energy absorption of nanoscale of uniform and gradient gyroid

From the stress-strain curve of Fig. 2(a), a nano-gyroid with a gradient from 0 to 4 all reached a dense state. Moreover, the energy

absorption per unit volume with a densification strain  $\varepsilon_d$  can be calculated according to Eq. (7),

$$W_{\nu} = \int_{0}^{\varepsilon_{d}} \sigma(\varepsilon) d\varepsilon, \tag{7}$$

where  $W_{\nu}$  is the cumulative energy absorption per unit volume for nano-gyroid structures,  $\varepsilon$  is the strain, and  $\sigma(\varepsilon)$  is the effective stress related to  $\varepsilon$  during the compression simulations. From Fig. 6(a), the smaller the structural gradient is, the longer the linear region of the curve is. With the increase of the structural gradient, it is seen the curvature of the relationship between energy absorption and strain becomes more nonlinear. This is because the structure with gradient 0 has a long plastic deformation region. Additionally, as the structural gradient increases, its dense cumulative absorption capacity gradually increases. The results show that the larger the gradient of nano-Gyroid structure is, the higher the

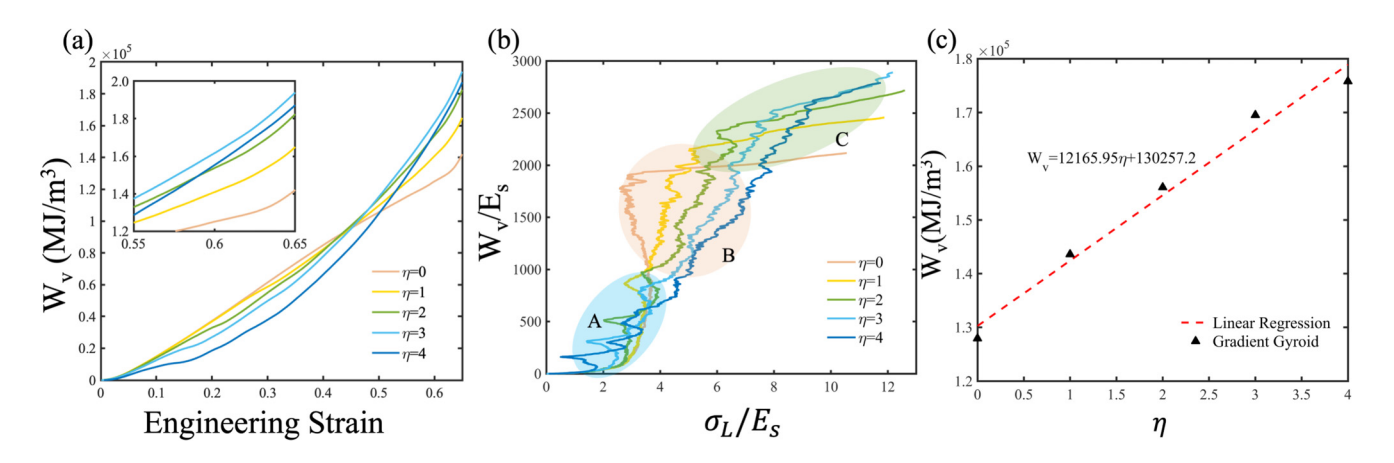


FIG. 6. (a) Cumulative energy absorption per unit volume vs strain curves; (b) normalized energy absorption of nano-gyroid structures with gradients 0 and 4, respectively; (c) the relationship between gradient and energy absorption.

**TABLE I.** Densification strains  $\varepsilon_d$  and energy absorbed per unit volume at densification  $W_v$  for the gradient nano-gyroid structures.

Type	$\eta = 0$	$\eta = 1$	$\eta = 2$	$\eta = 3$	$\eta = 4$
Strain $\varepsilon_d$	0.615	0.608	0.606	0.615	0.634
Energy absorbed $W_{\nu}(MJ/m^3)$	127 936.2	143 601.8	156 081.1	169 519.6	175 807.1
$W_{\nu}$ stainless steel <sup>31</sup>	16.21	N/A	N/A	16.60	16.82
$W_{\nu}$ , Lightweight polymer <sup>23</sup>	2.31	N/A	N/A	2.42	2.47

energy absorption capacity can achieve. Therefore, the gradient structure can provide greater strain protection before densification. Moreover, the numerical value shows that the cumulative energy absorption value of the nano-gyroid structure with a gradient of 4 is about 37.4% higher than that of a uniform structure with a gradient of 0 (Table 1). Furthermore, from Fig. 6(b), the dimensionless total effective stress of the gyroid structure increases rapidly with a slight gradient increasing when the energy absorption rises to a certain value (~1000). Overall, for structures with larger gradient, the total energy absorption ability increases much faster, therefore more conducive to buffer energy absorption. Noteworthy, roughly comparing to the traditional materials like lightweight polymer<sup>23</sup> and stainless steel,<sup>31</sup> the energy absorption of the nano graded gyroid is over 10 000 times higher, which indicates the exceptional energy absorption capability of this novel structure.

Moreover, as shown in Fig. 6(c), the relationship between the gradient of the nano-gyroid structure and the cumulative energy absorption value is established. It can be seen from the fitted result that there is an approximately linear relationship between the gradient change and the cumulative energy absorption. Therefore, a linear fitting equation can be established to predict the cumulative energy absorption corresponding to different gradients.

### IV. CONCLUSION

In summary, nanoscale gyroids with different gradients were designed, and their mechanical properties were characterized by MD simulation. Compared with the overall compressive deformation of a homogeneous nano-gyroid structure, the gradient structure is compressed hierarchically and densified layer by layer. Unlike the conventional Gyroid lattice, gradient gyroid lattice reveals a scaling of yield strength  $(\sigma_y)$  to the relative density  $(\rho')$  in the factor of 1.5, exhibiting a stretch dominant behavior yielding a much better mechanical property. Furthermore, the results show that as the gradient increases, the overall energy absorption value of the structure increases. Therefore, the relationship between the gradient level and energy absorption is established to predict energy absorption.

## **ACKNOWLEDGMENTS**

Funding for this research is provided by the National Science Foundation (NSF) under Award Nos. NSF-1826439 and NSF-1762792. Support from the National Natural Science Foundation of China (No. 52005261) is also greatly acknowledged. The authors acknowledge the Agave Computer Cluster of ASU for providing the computational resources.

### **AUTHOR DECLARATIONS**

#### **Conflict of Interest**

The authors declare that they have no known competing financial interests or personal relationships that could have appeared to influence the work reported in this paper.

### **Author Contributions**

R.D. and D.L. have contributed equally to this work.

Rui Dai: Conceptualization (equal); Data curation (equal); Project administration (equal); Writing – original draft (equal); Writing – review & editing (equal). Dawei Li: Data curation (equal); Methodology (equal); Validation (equal); Writing – original draft (equal); Writing – review & editing (equal). Wenhe Liao: Methodology (equal); Supervision (equal); Writing – review & editing (equal). Validation (equal); Writing – review & editing (equal). Yunlong Tang: Methodology (equal); Validation (equal); Writing – review & editing (equal). Qiong Nian: Conceptualization (equal); Funding acquisition (equal); Project administration (equal); Supervision (equal); Writing – original draft (equal); Writing – review & editing (equal).

### **DATA AVAILABILITY**

The data that support the findings of this study are available within the article.

### **REFERENCES**

- <sup>1</sup>B. D. Wilts, B. A. Zubiri, M. A. Klatt, B. Butz, M. G. Fischer, S. T. Kelly, E. Spiecker, U. Steiner, and G. E. Schröder-Turk, "Butterfly gyroid nanostructures as a time-frozen glimpse of intracellular membrane development," Sci. Adv. 3, e1603119 (2017).
- <sup>2</sup>J. Bauer, L. R. Meza, T. A. Schaedler, R. Schwaiger, X. Zheng, and L. Valdevit, "Nanolattices: An emerging class of mechanical metamaterials," Adv. Mater. 29, 1701850 (2017).
- <sup>3</sup>V. Luzzati and P. A. Spegt, "Polymorphism of lipids," Nature 215, 701 (1967).
- <sup>4</sup>Z. Gan, M. D. Turner, and M. Gu, "Biomimetic gyroid nanostructures exceeding their natural origins," Sci. Adv. 2, e1600084 (2016).
  <sup>5</sup>C. Pouya, J. T. B. Overvelde, M. Kolle, J. Aizenberg, K. Bertoldi, J. C. Weaver,
- <sup>5</sup>C. Pouya, J. T. B. Overvelde, M. Kolle, J. Aizenberg, K. Bertoldi, J. C. Weaver, and P. Vukusic, "Characterization of a mechanically tunable gyroid photonic crystal inspired by the butterfly parides sesostris," Adv. Opt. Mater. 4, 99 (2016).
  <sup>6</sup>E. Goi, B. P. Cumming, and M. Gu, "Gyroid 'srs' networks: Photonic materials beyond nature," Adv. Opt. Mater. 6, 1800485 (2018).
- <sup>7</sup>L. Lu, J. D. Joannopoulos, and M. Soljačić, "Topological photonics," Nat. Photonics **8**, 821 (2014).

- <sup>8</sup>S. Choudhury, M. Agrawal, P. Formanek, D. Jehnichen, D. Fischer, B. Krause, V. Albrecht, M. Stamm, and L. Ionov, "Nanoporous cathodes for high-energy Li–S batteries from gyroid block copolymer templates," ACS Nano 9, 6147 (2015).
- <sup>9</sup>M. M. Sychov, L. A. Lebedev, S. V. Dyachenko, and L. A. Nefedova, "Mechanical properties of energy-absorbing structures with triply periodic minimal surface topology," Acta Astronaut. 150, 81 (2018).
- <sup>10</sup>A. Ataee, Y. Li, M. Brandt, and C. Wen, "Ultrahigh-strength titanium gyroid scaffolds manufactured by selective laser melting (SLM) for bone implant applications," Acta Mater. 158, 354 (2018).
- <sup>11</sup>D. W. Abueidda, M. Elhebeary, C.-S. A. Shiang, S. Pang, R. K. Abs Al-Rub, and I. M. Jasiuk, "Mechanical properties of 3D printed polymeric gyroid cellular structures: Experimental and finite element study," Mater. Des. 165, 107597 (2019)
- <sup>12</sup>M. Pelanconi and A. Ortona, "Nature-Inspired, ultra-lightweight structures with gyroid cores produced by additive manufacturing and reinforced by unidirectional carbon fiber ribs," Materials 12, 4134 (2019).
- <sup>13</sup>L. R. Meza, S. Das, and J. R. Greer, "Strong, lightweight, and recoverable three-dimensional ceramic nanolattices," Science 345, 1322, (2014).
- <sup>14</sup>X. Zheng, H. Lee, T. H. Weisgraber, M. Shusteff, J. DeOtte, E. B. Duoss, J. D. Kuntz, M. M. Biener, Q. Ge, and J. A. Jackson, "Ultralight, ultrastiff mechanical metamaterials," Science 344, 6190, (2014).
- 15 J.-H. Park and J.-C. Lee, "Unusually high ratio of shear modulus to Young's modulus in a nano-structured gyroid metamaterial," Sci. Rep. 7, 10533 (2017).
- <sup>16</sup>J.-H. Park and J.-C. Lee, "Peculiar elastic behavior of mechanical metamaterials with various minimal surfaces," Sci. Rep. 9, 2941 (2019).
- <sup>17</sup>Z. Qin, G. S. Jung, M. J. Kang, and M. J. Buehler, "The mechanics and design of a lightweight three-dimensional graphene assembly," Sci. Adv. 3, e1601536 (2017).
- <sup>18</sup>A. Ataee, Y. Li, D. Fraser, G. Song, and C. Wen, "Anisotropic Ti-6Al-4V gyroid scaffolds manufactured by electron beam melting (EBM) for bone implant applications," <u>Mater. Des.</u> 137, 345 (2018).
- <sup>19</sup>S. N. Khaderi, V. S. Deshpande, and N. A. Fleck, "The stiffness and strength of the gyroid lattice," Int. J. Solids Struct. 51, 3866 (2014).

- <sup>20</sup>J. Li, J. Li, Q. Zhao, and R. Xia, "Molecular dynamics simulations on the mechanical properties of gyroidal bicontinuous Cu/Ni nanocomposites," J. Mater. Res. Technol. 18, 4738 (2022).
- <sup>21</sup>Y. Zhang, Y. Xian, J. Li, S. Ding, S. Liu, and R. Xia, "Atomistic investigation on the mechanical properties of 3D nanoporous metallic glasses under uniaxial tension and compression," Mater. Today Commun. 27, 102460 (2021).
- <sup>22</sup>S.-W. Lee, M. Jafary-Zadeh, D. Z. Chen, Y.-W. Zhang, and J. R. Greer, "Size effect suppresses brittle failure in hollow Cu60Zr40 metallic glass nanolattices deformed at cryogenic temperatures," Nano Lett. 15, 5673 (2015).
- <sup>23</sup>D. Li, W. Liao, N. Dai, and Y. M. Xie, "Comparison of mechanical properties and energy absorption of sheet-based and strut-based gyroid cellular structures with graded densities," <u>Materials</u> 12, 2183 (2019).
- 24S. Plimpton, "Fast parallel algorithms for short-range molecular dynamics," J. Comput. Phys. 117, 1 (1995).
- <sup>25</sup>Y. Mishin, M. J. Mehl, D. A. Papaconstantopoulos, A. F. Voter, and J. D. Kress, "Structural stability and lattice defects in copper: *Ab initio*, tight-binding, and embedded-atom calculations," Phys. Rev. B **63**, 224106 (2001).
- <sup>26</sup>R. D. Boyer, J. Li, S. Ogata, and S. Yip, "Analysis of shear deformations in Al and Cu: Empirical potentials versus density functional theory," Modell. Simul. Mater. Sci. Eng. 12, 1017 (2004).
- <sup>27</sup>L. J. Gibson, M. F. Ashby, G. S. Schajer, and C. I. Robertson, "The mechanics of two-dimensional cellular materials," Proc. R. Soc. London. A. Math. Phys. Sci. 382, 1782 (1982).
- <sup>28</sup>J. A. Baimova, B. Liu, S. V. Dmitriev, and K. Zhou, "Mechanical properties of crumpled graphene under hydrostatic and uniaxial compression," J. Phys. D: Appl. Phys. 48, 095302 (2015).
- 29 J. A. Baimova, B. Liu, S. V. Dmitriev, N. Srikanth, and K. Zhou, "Mechanical properties of bulk carbon nanostructures: Effect of loading and temperature," Phys. Chem. Chem. Phys. 16, 19505 (2014).
- 30X. Zhou, H. Zhou, X. Li, and C. Chen, "Size effects on tensile and compressive strengths in metallic glass nanowires," J. Mech. Phys. Solids 84, 130 (2015).
- <sup>51</sup>L. Yang, R. Mertens, M. Ferrucci, C. Yan, Y. Shi, and S. Yang, "Continuous graded gyroid cellular structures fabricated by selective laser melting: Design, manufacturing and mechanical properties," Mater. Des. 162, 394 (2019).